JJMIE

Volume 17, Number 1, March. 2023
ISSN 1995-6665
Pages 127 – 138

Jordan Journal of Mechanical and Industrial Engineering

Dynamic Modeling of the Dog Clutch Engagement Process Using Hybrid Automata

Ayham Aljawabrah*, Laszlo Lovas

Department of Railway Vehicles and Vehicle-System Analysis, Faculty of Transportation Engineering and Vehicle Engineering, Budapest University of Technology and Economics, Sztoczek u. 2., 1111 Budapest, Hungary

Received 23 Aug 2022 *Accepted 14 Jan 2023*

Abstract

A detailed system dynamics model is essential for the design and calibration of the system controller. This paper introduces a control-oriented full dynamic model for the dog clutch engagement process that can be integrated with other system dynamic models found in ground vehicle transmission systems, such as the shifting mechanism system. This integrated model can be used later to design a position controller of the shifting mechanism's linkages to achieve a successful gearshift process. The engagement process is divided into four main stages, each of which has distinct dynamic behavior. The dynamics of each discrete stage are analyzed and modeled, and then, the discrete stages are integrated into one model using the hybrid automata modeling technique. Hybrid automata enables us to describe the continuous states within the discrete stages, which is better than continuous time techniques. The possible interactions between the sliding sleeve and the gear are analyzed and based on these interactions, the transition paths' conditions between these stages are established. The hybrid automata model comprises four discrete stages and ten guards that govern the transition between these stages. This model was simulated using Simulink State flow. Three cases are considered to verify the model, and the results showed that it could accurately capture the continuous system dynamics despite four discrete states. Furthermore, the transitions between the discrete states match the possible transition paths and guards.

Keywords: Dog clutch dynamics, shiftability, Hybrid automata, Gearshift, Simulink, Stateflow.

Nomenclature

ξ	relative angular position
ξ_0	initial relative angular position
$\Delta\omega$	mismatch speed
x_s	linear position of the sliding sleeve
x_0	axial gap
v_0	mean linear (axial) velocity
x_{fed}	overlap distance
Z	teeth number
r	mean radius of the dog clutch
h_t	tooth height
ϕ	angular pitch
ϕ_t	angular tooth thickness
Φ_b	angular backlash
m	mass of the shifting mechanism
J	inertia
θ	angular position
k	stiffness coefficient
d	damping coefficient
F_{act}	actuator force
T_c	side (tangential) impact torque
F_c	front (axial) impact force
HA	hybrid automaton
CA	continuous time
t	time

Subscripts

g	meshing gear (input side)
s	sliding sleeve (output side)
s,i	initial linear position
s,f	final linear position
$s,0$	linear face impact position

1. Introduction

Nonrenewable fuel shortages and environmental problems are becoming increasingly pressing global issues, leading the world to turn towards renewable energy sources[1, 2], and clean, efficient system[3]. As a result, motor vehicles are receiving more attention for their efficiency and ability to adopt clean energy concepts, as nonrenewable fuels traditionally power them.

Motor vehicles can be cleaner for the environment by improving engine efficiency or using alternative fuels. Mallouh [4] studied the usage of the fuel cell (FC) in rickshaws (three-wheeled vehicles) rather than conventional internal combustion engines (ICE), where these vehicles are widely common in the Asian urban environment. The significance of FC vehicles is the zero CO_2 emissions compared to conventional ICE. Their study

* Corresponding author e-mail: aaljawabrah@edu.bme.hu.

used two configurations: low-power fuel cell (LP FC) and high-power fuel cell (HP FC). They claimed LP FC was better than the conventional model by 57% and 58%, respectively, in the daytime drive cycle. Liu[5]performed an experimental study on using alcoholic fuel instead of conventional gasoline. His study focused on methanol as an alcohol fuel, and the research goal was to study the formaldehyde emissions -unconventional emissions- where they tend to have a higher concentration in alcohol fuels. He found that among there methanol fuels studied, the combustion characteristics and combustion speed of M85 methanol gasoline are similar to that of RON93 gasoline, so, this fuel can be used as fuel for ignition engines and has good energy-saving and environmental protection characteristics.

Another key component that can improve the vehicle's efficiency is the vehicle transmission. The development of motor vehicles began with the introduction of internal combustion engines (ICEs) and the need for a multi-gear ratio transmission. The synchronizer's invention allowed a mechanism to shift between these different gear ratios. The synchronizer is studied by many researchers [6-8]. The synchronizer lasted for many decades as the gearshift mechanism, but the fuel shortage and the environmental issues caused the need for a more efficient system since the synchronizer employs friction for input-output speed synchronization and has a large mass. Dog teeth clutch has been replacing the synchromesh because it provides quicker shifting time, simpler structure, larger power transmitting capacity, and has lower cost[9, 10]. Also, It has excellent potential in ICE and electric vehicles (EV).

The use of a friction-based mechanism to align the speeds of the input and output sides of the gearbox limits the lifespan of the synchronizer. However, the speed synchronization mechanism needs a long service life for heavy-duty- or commercial-vehicles. As a result, the synchronizer cannot be widely used in heavy-duty vehicles due to the limitations of materials strength and manufacturing technology[11, 12]. Automatized manual transmission (AMT) has been used in heavy-duty vehicles due to its great transmission torque, high transmission efficiency, and low manufacturing and maintenance costs[13, 14]. AMT employs the dog clutch as a shifting element, but as it is only a clutch and not a synchronizer, the problems of synchronization shall be studied, and many authors studied the gearshift process in AMT[15-17]. Bóka[16] described an external synchronization strategy for a dog clutch in automatized mechanical transmission (AMT) for heavy-duty commercial vehicles. Later, Bóka[18] developed more the strategy. He used a dynamic modeling approach for system modeling and used the notion of engagement probability to find a certain successful gearshift region. In his work, he considered the initial angular relative position random in the interval $[0,\phi]$, which denotes one pitch period of the gear's tooth. Thus, he needed to develop a strategy that guarantees a successful gearshift despite the system uncertainty. He developed a dynamic model and, based on the initial mismatch speed, he developed a probability equation. During the face contact phase of the clutch engagement, a friction torque exists which reduces the mismatch speed. His model assumed that the teeth have infinite width and can contact until the mismatch speed vanishes. He defined the variation in the relative angular position φ_{ff}, from the contact starting with face friction until the mismatch speed vanishes and observed that it depends on the initial mismatch speed. Then he defined the probability as the ratio $(\varphi_{ff+}\ \Phi_b)/\phi$ with a maximum value of 1. For a given dog clutch geometry, he found that the engagement probability depends on the gear ratio. Further on, he found that if them is match speed is above a threshold, there is a certain successful gearshift. He validated the analytical probability calculation with experimental statistical study, and the analytical probability agreed with the experimental results. However, this concept of the available relative rotation, φ_{ff}, is applicable only for the low mismatch speed region.

Jasný[19] presented a multi-body simulation model in Adams software that is created to minimize the gearshift time based on the dogs' shape, and validated the simulation model using measurements of a prototype dog clutch. The prototype has positive tapers of the dog sides. In the experiments, high mismatch speeds up to 249 RPM are applied, and it showed that the gearshift time reduces with higher RPM and gearshift force. He applied a time-varying force profile in the simulation and considered different engagement cases. Among these cases, a successful gearshift without face impact case is used for this work validation. The prototype's geometry in[19] is adapted to match the considered geometry in this work, as described in chapter 4 of this manuscript.

In the case of electric vehicles, the battery range for an EV during city operation can be reduced by increasing the speed of the electric motor (EM) through a high transmission ratio to increase EM efficiency. Multi-speed battery electric vehicles (BEV) can be used for the reduction of electric consumption[20, 21] and the downsizing of the EM[22, 23]. EV employs clutch less AMTs where the friction cone is removed, and the speed synchronization is achieved by electric motor control [24-27]. Eßer[28] analyzed the potential energy savings of different BEV concepts in urban driving. He used backward facing implementation of the longitudinal vehicle dynamics and found that "Two-Drive-Transmission" (TDT) reduced electric consumption. Some researchers went further in improving the performance and efficiency of EV gearboxes. Zhang[29] performed contact mechanics analysis and optimization of the gear tooth shape's profile modification. Pan[30]studied the mechanical vibration caused by electromechanical coupling of alternating current (AC) Asynchronous Motor Drive System

The dog clutch application faces problems regarding synchronization and gearshift control, which requires accurate dynamic modeling of the gearshift process to study the system thoroughly.

This work shows that the dog clutch operation has four discrete and several continuous states. To model the behavior, continuous-time (CT) modeling techniques were used, but this requires modeling the discrete states' dynamics and the transition guards within one model, which has many drawbacks. The model complexity increases, as well as the simulation time, since unnecessary dynamics for various discrete states will be evaluated. After the dynamics of all states are evaluated, their effect on the continuous states is included only if a specific condition is satisfied. In contrast, using hybrid automata (HA) techniques, the state dynamics and the transition guards are modeled separately, and only the current state dynamics are evaluated.

HA theory is discussed in several literatures[31-34]. It consists of discrete states, a set of transition paths, and a set of guards, one for each path. Hybrid automata modeling is an efficient technique to model a dynamic system with several discrete states to capture its continuous variables' trajectories. It is widely used in dynamic modeling and control of vehicle powertrain and gear shifting.

Fu[35], presented a scheme of hybrid modeling of an integrated motor-transmission powertrain used in electric vehicles to analyze its performance. He developed a motor automaton and a gearbox automaton that describe the hybrid property of subsystems presented. The gearbox and motor have several discrete states. HA model was created for the motor, gearbox, and the rest of the system. The model has three main stages: the first gear engaged, then disengaged, and finally, the second gear engaged. The model captured all possible actions during the vehicle operation. The simulation results showed the effectiveness of the proposed model for both upshift and downshift since it reflected precisely the profiles of torque and speed. Chen and Mitra[36] synthesized a controller for the meshing process of a Motor-Transmission Drive powertrain for electric vehicles with uncertain initial states. They verified the safety property concerning the continuous-time hybrid automata (CHA) model for the trajectory of the sleeve during the meshing process to guarantee that the meshing time is within a bounded time at every initial state. They used the CHA model to solve an optimal control problem, and the synthesized controller could reduce the meshing duration by 71.05% and reduce impact impulse by 85.72% compared to an existing controller. Lu[37] designed a control strategy for non-synchronizer electric-driven mechanical transmission (EMT). He developed a HA model for the gear shifting process and showed that the impacts could be avoided by achieving both zero relative rotational speed and zero angle differences between the sleeve and clutch gear. Simulations and bench tests were carried out to validate the control strategy, and the control strategy reduced the impacts and power-off time. Yuanfan[38] presented a non−synchronizer motor−transmission drive system. He developed a HA model to describe the gear change process at each stage. Based on the dynamic characteristics of each stage, he developed a control strategy with active synchronization for both the rotational speed difference and relative angular speed between the sleeve and the meshing gear. The simulation and experimental validation showed that the developed model can simulate the actual process, and the results showed that this control strategy provides a fast and impact-free gearshift while the power interruption time was reduced to 350 ms.

According to the literature review, dynamic models are necessary for studying and designing controllers for dog clutches. Experimental test rigs, similar to those described in [39, 40], are also necessary for calibrating and validating these dynamic models. Our work focuses on the dynamic modeling of the dog clutch engagement process to create a control-oriented standard dynamic model. This model can be easily integrated with other dynamic models in the vehicle's transmission and used for controller design and calibration of the gearshift process. To develop such a dynamic model, it is essential to understand the system and the possible interactions between system components and the conditions for impact detection. Therefore, this work aims to:

1. Describe the dynamic engagement process of the dog clutch.
2. Introduce the main engagement process stages.
3. Establish the possible transition paths between the discrete stages and the transition conditions for each path.
4. Describe the dynamics of each stage and introduce the impact models.
5. Introduce the Hybrid automata model to describe the states' continuous dynamics based on the discrete stages and the transition guards.

2. Dog clutch geometric model

2.1. Dog clutch

A dog clutch is a coupling used to transmit power. It consists of two parts having complementary geometry. These complementary shapes are referred to as dog teeth. Teeth can be present either on the circumference of a cylinder (radial clutch or spline clutch) or on the circular surface of the cylinder (axial clutch or face clutch). Radial dog teeth clutches are traditionally used for power transmission in automotive gearboxes (cars, trucks, buses), as a part of the synchronizer. Axial dog teeth clutches are traditionally used for power transmission in motorbike gearboxes, where the torque is much less than in a truck case. In this study, axial dog teeth clutches are considered. However, the described method can be applied independently of the place of the geometry.

Let us consider a dog teeth clutch composed of an axially moving part called a sliding sleeve and an axially fixed but rotating part called the meshing gear. The coupling is realized by the axial motion of the sliding sleeve(Figure 1).

Figure 1. Face dog clutch

The main geometry parameters are presented in Table 1. The dog geometry is shown in Figure 2. At the beginning of the shifting, the sliding sleeve (s) and the meshing gear (g) have an axial gap x_0 and initial relative angular position ξ_0 between the marked red teeth. The sliding sleeve can slide axially while it has relative angular rotation with respect to the target gear. The relative angular rotation is called the mismatch speed $\Delta\omega$. The engagement of the complementary geometries is eased with an angular backlash Φ_b.

Table 1. Dog clutch shiftability parameters

Parameter	Unit	Parameter	Unit
ξ	[º]	x_0	[mm]
Z	[-]	x_{fed}	[mm]
F_{act}	[N]	Φ_b	[º]
$\Delta\omega$	[rad] ([min^{-1}])		

The axial dog clutch has an angular pitch ϕ given by Eq. (1) and an angular backlash given according to Eq. (2), where ϕ_t is the tooth thickness angle:

$$\phi = \frac{2\pi}{z} \quad (1)$$

$$\Phi_b = \phi - 2\phi_t \quad (2)$$

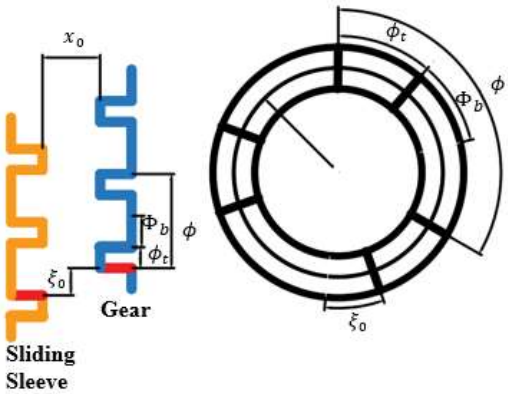

Figure 2. Dog clutch geometry

The angular relative position ξ between the sliding sleeve and the meshing gear is defined according to Eq. (3):

$$\xi = \theta_g - \theta_s \quad (3)$$

During the engagement process, a tooth on the gear can pass many teeth on the sliding sleeve, so that, a dotted orange line is used in Figure 3c, d, and f to indicate that many teeth are included in this area. The value of ξ can be much larger than ϕ, so, it should be transferred to the first cycle (or between [-ϕ, ϕ]) according to Eq. (4).Here ,ξ' is the relative position in the first cycle and measured between the red-marked edge on the meshing gear and green-marked edge on the sliding sleeve shown in Figure 3b. Also, the same angular position reference can be seen in Figure 3d as 3D view, where the red and green edges are seen as red and green faces, respectively.

$$\xi' = mod(\xi, \phi) \quad (4)$$

ξ' can have negative values, and it is more appropriate for some analysis cases to transfer it to the positive first cycle or in the interval [0, ϕ].This can be achieved according to Eq. (5).

$$\xi'^{+} = \xi' + \frac{1 - sign(\xi')}{2}\phi \quad (5)$$

The term $((1\text{-}sign(\xi'))/2)$ guarantees that ξ' is transferred to the positive first cycle only when it is negative. The mismatch speed is defined according to Eq. (6):

$$\Delta\omega = \dot{\theta}_g - \dot{\theta}_s \quad (6)$$

3. Modeling of the engagement process

The dog clutch passes several stages during the gearshift process. The following figures illustrate the engagement stages, and the sliding sleeve and the meshing gear interaction possibilities are discussed. Then, the impact model is presented. Afterward, a HA model for the engagement process is presented.

3.1. Presentation of the engagement process

The engagement process can be divided into four main stages, 1) free fly axial motion, 2) axial (face) impact stage, 3) tangential (side) impact stage, and 4) full engagement stage.

Between the sliding sleeve and the meshing gear, there exists a mismatch speed $\Delta\omega_0$ and an axial gap x_0 (Figure 3a). Also, an initial angular relative position ξ_0 exists between the red-marked edges in Figure 3a, or between the red-marked faces in Figure 3b. The engagement of the dog clutch is realized by the axial motion of the sliding sleeve. At the beginning of the shifting at t_0(Figure 3a), the constant actuator force F_{act} moves the sliding sleeve axially until the axial gap is removed at t_1. During this time, the dog clutch parts rotate relative to each other, and the relative angular position changes from ξ_0 to ξ_1, as seen in Figure 3c and Figure 3d.

At the beginning of stage 2, the sleeve and gear teeth meet at the face impact position x_0 (or $x_{s,0}$), and a face (or axial impact) occurs between the sliding sleeve and the meshing gear sleeve teeth' as shown in Figure 3c. This impact is accompanied by face friction which reduces the mismatch speed, as seen from $\Delta\omega$ curve in Figure 4, stage 2. The sliding sleeve can continue moving axially, or it may stop for a period as the curve for x_s (Figure 4).The face impact is possible to occur until the overlap x_{fed} distance is covered at t_2 (Figure 3e). We suppose that if a tooth on the sliding sleeve can overlap a tooth on the meshing gear sleeve, the sliding sleeve will not bounce back, and a successful engagement is guaranteed. This distance is called overlap and noted x_{fed}. While reaching the overlap, a relative rotation between the dog clutch and the target gear occurs, and the relative angular position changes from ξ_1 to ξ_2.

At stage 3, the sliding sleeve moves axially until it covers the full tooth height, at x_0+h_t(or $x_{0,f}$), in the axial direction, (Figure 3f). During this stage, the $\Delta\omega$ curve in Figure 4 shows the mismatch speed alternating around zero until it is reduced to zero. This speed synchronization results from the several side (or tangential) impacts between the sliding sleeve and the meshing gear sleeve teeth's sides.

Stage 4 ends the gearshift process, where the mismatch speed is synchronized, and the sliding sleeve reaches the final axial position x_0+h_t.

At the end of stage 1, the sliding sleeve can continue to stage 2 and freely pass through without impacting the sleeve, Figure 5a, or firstly, it impacts the meshing gear sleeve, Figure 5b and c.

If the impact happens, contact occurs between the gear and sleeve teeth, which initiates bounce back and friction forces. The sliding sleeve can bounce back or stick to the gear. The bounce back or stick behavior depends on the contact model parameters, i.e., whether the system is under- or over-damped. The sleeve can impact the gear and stop moving, then continues the axial motion when the next gap on the meshing gear is reached(Figure 5b). Moreover, a tooth on the sliding sleeve can impact many teeth on the meshing gear before it can continue the axial motion (Figure 5c). These impacts cause friction between the sleeve and the gear' faces that reduce the mismatch speed and make the engagement possible. Finally, a tooth on the sliding sleeve can keep impacting each passing tooth on the meshing gear, but it cannot pass through. This happens if the mismatch speed is very large, and the applied actuator force is not large enough to move the sleeve and cover the overlap distance before the next tooth on the gear is reached.

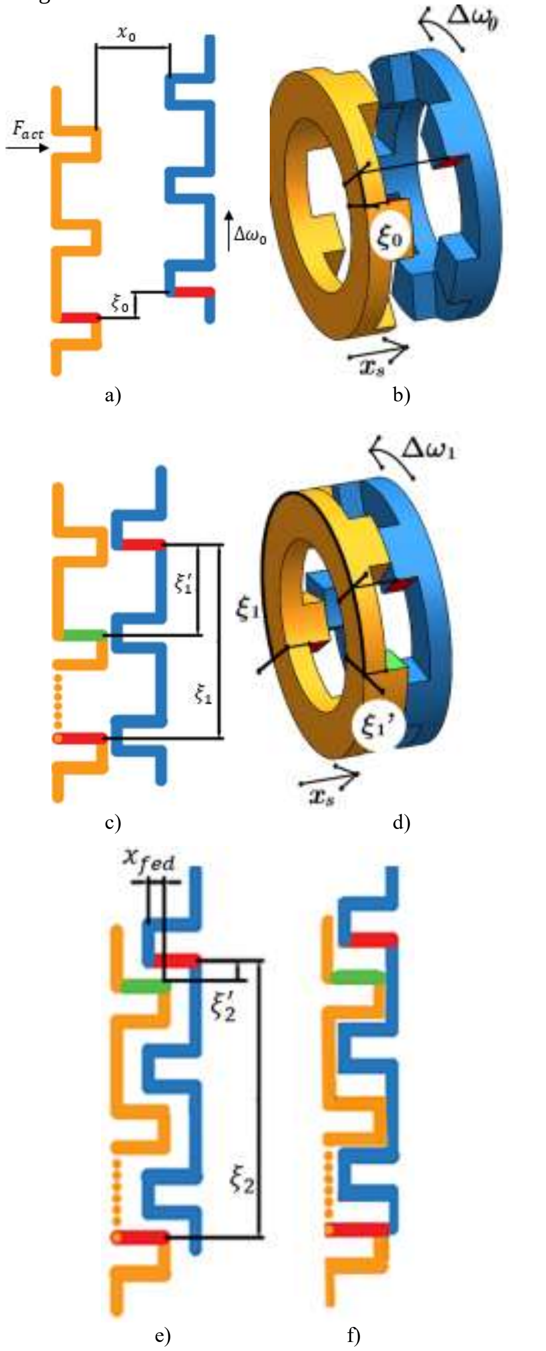

Figure 3. Schematics of dog clutch engagement stages at the beginning of: stage 1 in a) 2D and b) in 3D, stage 2 in c) 2D and d) in 3D, e) stage 3, and f) stage 4

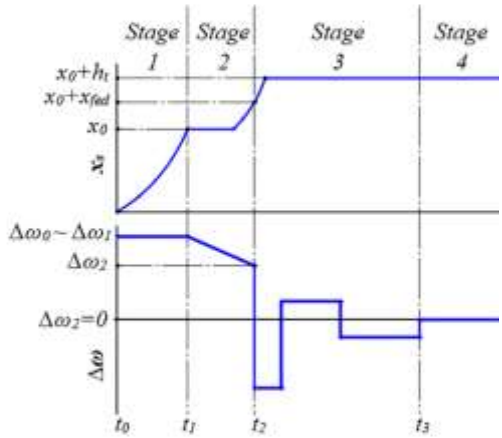

Figure 4. Dynamics of dog clutch engagement

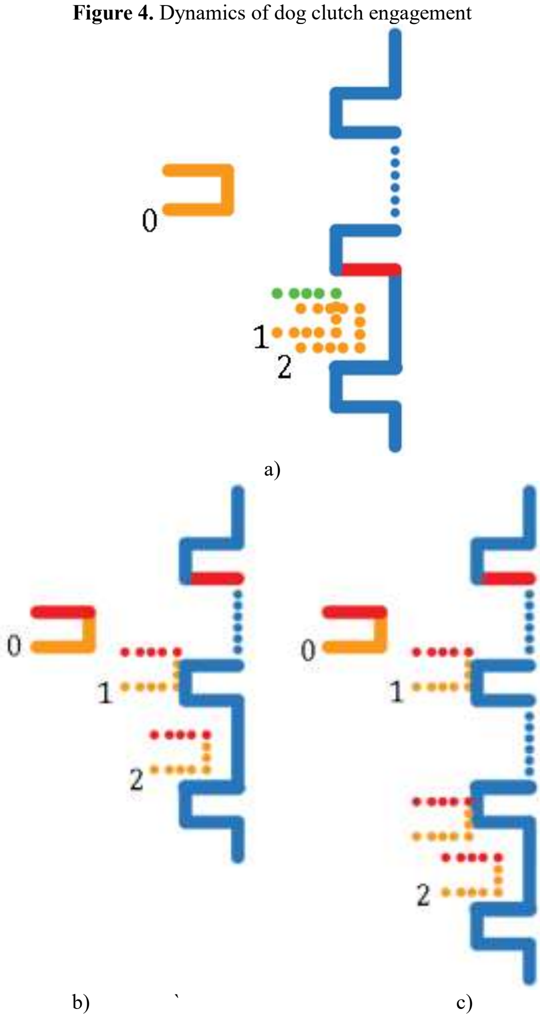

Figure 5. Possible sliding sleeve and the gear interactions

The condition to have a free impact engagement process can be developed for four different configurations based on the sign of the mismatch speed and the relative position, as shown in Fig. 6.

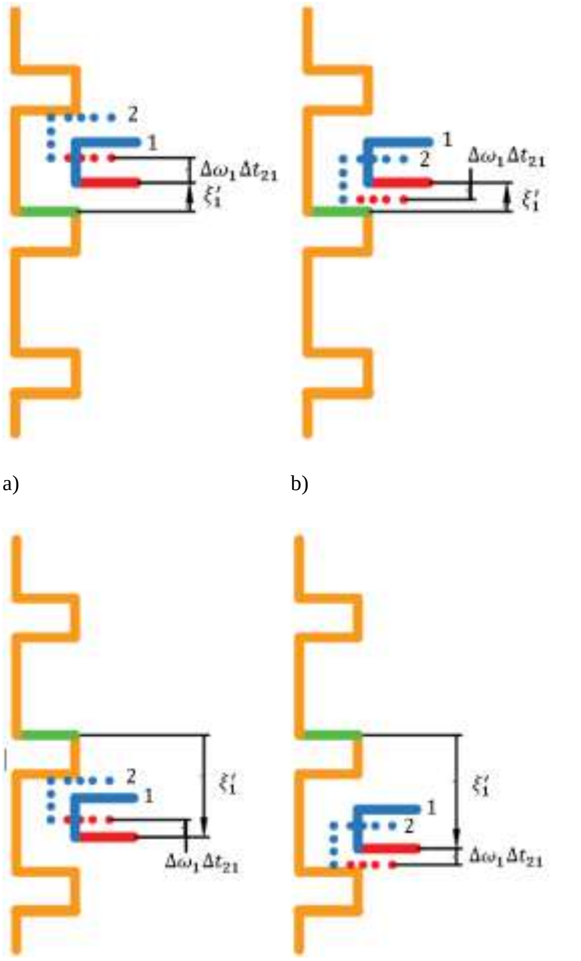

a) b) c) d)

Figure 6. Free face impact engagement possible cases: a) *$\Delta\omega_0>0$ and $\xi_1'>0$*,b) *$\Delta\omega_0<0$ and $\xi_1'>0$*,c) *$\Delta\omega_0>0$ and $\xi_1'<0$*,d) *$\Delta\omega_0<0$ and $\xi_1'<0$*

The time to cover the overlap distance t_{21} is short, so the mismatch speed is assumed to be constant during this time since the gearbox losses can be ignored. Based on this assumption, the four conditions can be derived. In Fig. 6a, after the sleeve covers the axial gap, it has to cover the overlap distance before the next tooth on the meshing gear sleeve is reached. In other words, ξ_1'plus the relative position change during the overlap distance coverage ($\Delta\omega_1 \cdot t_{21}$) should be less than the backlash Φ_b. According to this analogy, Eq. (7) can be derived. With the same analogy and with the aid of Fig. 6b-c, Eq. (8)-(10) can be derived respectively.

$$\xi_1' \le \Phi_b - \Delta\omega_1 \cdot t_{21}, \quad \Delta\omega_1 \ge 0 \wedge \xi_1' \ge 0 \tag{7}$$

$$\xi_1' \ge -\Delta\omega_1 \cdot t_{21}, \quad \Delta\omega_1 \le 0 \wedge \xi_1' \ge 0 \tag{8}$$

$$\xi_1' \le -(\phi - \Phi_b) - \Delta\omega_1 \cdot t_{21}, \quad \Delta\omega_1 \ge 0 \wedge \xi_1' \le 0 \tag{9}$$

$$\xi_1' \ge -\phi - \Delta\omega_1 \cdot t_{21}, \quad \Delta\omega_1 \le 0 \wedge \xi_1' \le 0 \tag{10}$$

$$t_{21} = \sqrt{\frac{m \cdot x_{fed}}{F_{act}}} \tag{11}$$

Eq. (9) and (10) can be transformed to Eq. (7) and (8), respectively, by transforming all angles to the positive first cycle using Eq. (5). The four conditions are now reduced to only two, Eq. (12) and (13). This simplification is important for building the HA model.

$$\xi_1'^{+} \le (\Phi_b - \Delta\omega_1 t_{21}) \wedge \Delta\omega_1 \ge 0 \tag{12}$$

$$\xi_1'^{+} \ge -\Delta\omega_1 t_{21} \wedge \Delta\omega_1 < 0 \tag{13}$$

For a given dog clutch geometry, the interaction possibilities between the gear and sleeve depend mainly on the initial relative position, the initial mismatch speed (or the mismatch speed at the end of the free fly stage), and the actuator force.

3.2. Impact model

The impact between two bodies is described using different models, such as the coefficient of restitution or the spring-damper model[41]. The latter is widely used in the literature[42, 43] and is employed here. Let's consider two moving blocks, as in Figure 7a, and then they impact, as in Figure 7b.

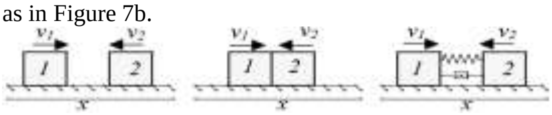

a) b) c)

Figure 7. Spring-damper impact model

During impact, the blocks are considered rigid, and a spring and a damper are assumed between them, as in Figure 7c. The contact force is given according to Eq.(14), where *k* is the spring constant and *d* is the damping coefficient. Assuming the contact force only acts on the blocks, the force balance for blocks 1 and 2 are given according to Eq.(15) and Eq.(16), respectively. In case of impact in rotational motion, equations of similar structure can be used.

$$F_c = k(x_1 - x_2) + d(v_1 - v_2) \tag{14}$$

$$m\ddot{x}_1 = -F_c \tag{15}$$

$$m\ddot{x}_2 = F_c \tag{16}$$

Once the impact forces (or torques) are known, it is important to find system-related conditions that detect a potential impact. Therefore, it is necessary to understand the behavior of the system and the possible interactions between its components. In what follows, we aim to identify the interactions between the gear and the sliding sleeve and establish the conditions for these interactions to occur. This is one of the main contributions of this work, since the limit conditions are essential to integrate the discrete states into one model.

The nature of the face impact depends on the sign of the initial relative position ξ' at the end of stage 1,while the side impact depends on both the sign of the relative position ξ' and the mismatch speed.

Firstly, l et's consider the axial impact. Figure 8 illustrates the axial impact cases. When the relative positionis positive, the impact configuration is shown in Figure 8a. The impact happens between the black-marked teeth if the relative position ξ' is between Φ_b and ϕ. However, Figure 8b shows that when the relative position is negative, the impact happens when ξ' is between $-2\phi_t$(or $-(\phi - \Phi_b)$) and *0*. These two conditions are summarized in Eq.(17) and (18). Eq. (18)can be transformed to Eq. (17)by expressing it in the positive first cycle, so, only one condition is required. This transformation is necessary for building the HA model. The impact force is given according to Eq.(19):

$$\Phi_b \le \xi' \le \phi, \tag{17}$$

$$-(\phi - \Phi_b) \le \xi' \le 0 \tag{18}$$

$$F_c = \begin{cases} k(x - x_0) + d\dot{x}_s, & \Phi_b \le \xi'^{+} \le \phi \\ 0 & elsewhere \end{cases} \tag{19}$$

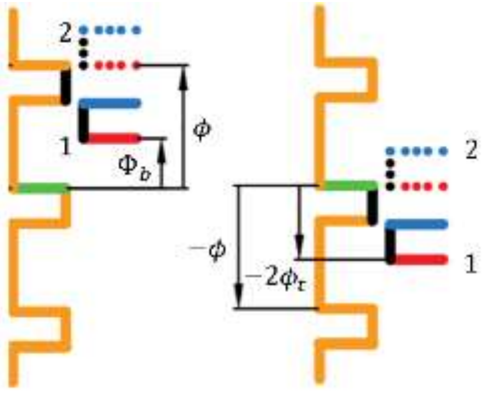

a) b)

Figure 8. Possible face impact configurations

Now let's consider the side impact cases shown in Figure 9. Firstly, consider the case when the mismatch speed and the initial relative position are both positive, as shown in Figure 9a. The impact happens when the relative position ξ' is larger than the backlash Φ_b. If the relative position is negative, there are two possible impact possibilities. firstly, when the mismatch speed is positive, case I in Figure 9b shows that the impact occurs if the relative position is between $-2\phi_t$ (or $-(\phi - \Phi_b)$) and 0. If the mismatch speed is negative, case II in Figure 9b shows that the impact happens when the relative position reaches zero. According to these conditions, the impact model is given according to Eq. (20).

$$T_c = \begin{cases} k_t(\xi' - \Phi_b) + d_t\Delta\omega\,, & \sigma_1 \\ k_t\big(\xi' - (\,\phi\, -\, \Phi_b)\big) + d_t\Delta\omega\,, & \sigma_2 \\ -k_t\xi' + d_t\Delta\omega\,, & \sigma_3 \\ 0\,, & \sigma_4 \end{cases} \tag{20}$$

$$\sigma_1 = \Phi_b \le \xi' \le \phi \;\wedge\; \Delta\omega \ge 0$$
$$\sigma_2 = -(\phi\, -\, \Phi_b) \le \xi' \le 0 \;\wedge\; \Delta\omega \ge 0$$
$$\sigma_3 = -(\phi\, -\, \Phi_b) \le \xi' \le 0 \;\wedge\; \Delta\omega \le 0$$
$$\sigma_4 = -\phi\; \le \xi' \le -(\phi\, -\, \Phi_b) \;\wedge\; 0 \le \xi' \le \Phi_b$$

This model should be simplified to simplify the HA model. Figure 9a shows a possible side impact if the ξ' is between Φ_b and ϕ. Also, Figure 9b shows that there is a side impact if the ξ' is between $-(\phi - \Phi_b)$ and 0. According to this, the side impact model is simplified according to Eq. (21).

Here, ξ'^0 refers to the angular position at the begging of the impact, so, ξ^0 can be $-(\phi - \Phi_b)$, or Φ_b for $\Delta\omega_0>0$, and 0 for $\Delta\omega_0<0$.

$$T_c = \begin{cases} k_t(\xi' - \xi^0) + d_t\Delta\omega & \sigma_1 \\ 0 & elsewhere \end{cases} \tag{21}$$

$$\sigma_1 = \Phi_b \le \xi' \le \phi \vee -(\phi\, -\, \Phi_b) \le \xi' \le 0$$

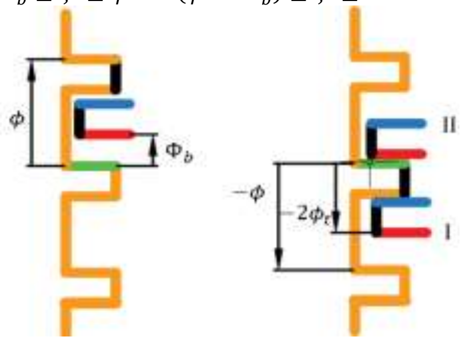

a) b)

Figure 9. Possible side impact configurations

3.3. Hybrid Automaton Model

Sections 3.1 and 3.2 introduced the main stages of the engagement process and impact models for both face and side impacts. There are four discrete states in the engagement process, but they can be integrated into a continuous hybrid automaton (HA) model to track the trajectory of the sleeve and gear during the engagement process.

Hybrid systems are digital real-time systems embedded in analog environments. One example of a hybrid system is a digital embedded control program for an analog plant environment, like a furnace or an airplane. The controller state moves discretely between control modes, and in each control mode, the plant state evolves continuously according to physical laws. These systems combine discrete and continuous dynamics [32]. Many mechanical systems are hybrid systems, such as a falling or bouncing ball. During the falling state, the dynamic behavior is governed by gravity and air resistance forces, while once the ball reaches the ground, impact forces become dominant. By combining these two discrete states in one analog environment, we can track the trajectories behavior of the bouncing ball- or the x- and y-position of the ball.

In what follows, we aim to formulate the dog clutch system in the HA system mathematically. A hybrid automaton H is a tuple of the form⟨ Loc, Edge, $\boldsymbol{X}$, Init, Inv, Flow, Jump⟩[32]. Here:

- Loc is a finite set [l_1, l_1, . . . l_n] of discrete locations. The dog clutch system has four discrete states, (l_1, l_2, l_3, l_4), where $l_1$refers to the free fly state, l_2 to the face impact state, l_3 to the side impact state, and l_4 for the full engagement state.
- Edge is a finite set of labeled edges representing the discrete changes of system behavior's mode in the hybrid system. The transition between two different states l_i and l_j, when ($i\neq j$) along these edges, or paths, is governed by a guard (g) accompanying each path, and these paths and guards usually have the same names. Based on the possible interaction between the gear and the sliding sleeve described in sections 3.1 and 3.2, we developed our system paths and their guard, summarized in Table 2. Our system has a set of ten edges [g_1, g_2, g_3, g_4, g_5, g_6, g_7, g_8, g_9, g_{10}]. The discrete states (l_1, l_2, l_3, l_4) are integrated using these ten edges according to Figure 10.
- $\boldsymbol{X}$ is a finite set [x_1, x_1, . . .,x_m] of real-valued variables. We use$\dot{X}$ for the set of dotted variables [$\dot{x}_1$, $\dot{x}_1$, . . .,$\dot{x}_m$], which represent the first derivatives of the variables during continuous evolutions (inside a discrete state). The system has two components: the meshing gear, which has only angular motion with the continuous state θ_g, and the sliding sleeve, which has angular and linear motions with continuous states (θ_s, x_s). From this, the continuous states of the model is$\boldsymbol{X}$= $(\theta_g, \theta_s, x_s)$ and their derivatives are $\dot{\boldsymbol{X}}$= $(\dot{\theta}_g, \dot{\theta}_s, \dot{x}_s)$.
- Init, Inv, Flow are functions that assign three predicates to each location. Init(l) is a predicate whose free variables are a subset of$\boldsymbol{X}$ which states the possible values for those variables when the hybrid system starts from location l. Inv(l) is a predicate whose free variables are from $\boldsymbol{X}$ and it constrains the possible valuations for those variables when the hybrid system

is in location l. Flow(l) is a predicate whose free variables are from $\boldsymbol{X} \cup \dot{\boldsymbol{X}}$, which states the possible continuous evolutions when the hybrid system is in location l. For the states l_1, l_2, and l_3 there are no restriction on the continuous states so Flow(l_1, l_2, l_3) is $[\theta_g, \theta_s, x_s, \dot{\theta}_g, \dot{\theta}_s, \dot{x}_s]$, while Inv($l_1$, l_2, l_3) is [ ], the empty set. However, some researchers such as[35] use the invariant $i_g=0$- or zero gear ratio- to indicate that the input (gear) and the output (sleeve) are disconnected, which is the case for l_1, l_2, and l_3. For l_4, the dog clutch reaches full engagement, where there is no further change in the linear position, and the angular speeds are synchronized or equal. From this, Inv(l_4) is $[\theta_g, x_s, \dot{\theta}_g, \dot{x}_s]$, where the gear angular position and speed are restricted by the sliding sleeve angular position and speed, respectively. Further on, Flow(l_4) is $[\theta_s, \dot{\theta}_s]$.

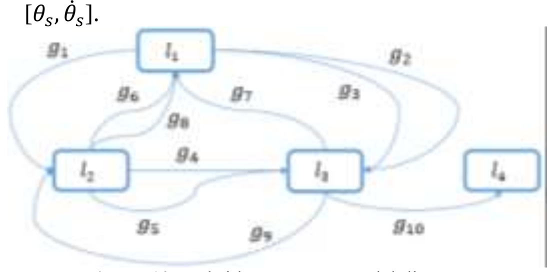

Figure 10. Hybrid automaton model diagram

After the discrete states and transition paths with their guards have been identified, it is essential to describe the dynamics within each discrete state. Here, the output side (sleeve) inertia is considered much larger than the input side (gear) inertia to simulate real-world vehicles.

Table 2. Invariants and guards

Invariants set	Guards
$I_1 \triangleq \{\boldsymbol{x} \mid i_g = 0$	$g_1 \triangleq x_0 \le x_s \le x_0 + x_{fed} \wedge \Phi_b \le \xi'^{+} \le \phi$ g_2: Eq. (12) $\wedge\ x_0 \le x_s \le x_0 + x_{fed}$ g_3: Eq. (13) $\wedge\ x_0 \le x_s \le x_0 + x_{fed}$
$I_2 \triangleq \{\boldsymbol{x} \mid i_g = 0$	$g_4 \triangleq x_s \ge x_0 + x_{fed} \wedge \Phi_b \le \xi' \le \phi \wedge \Delta\omega \ge 0$ $g_5 \triangleq x_s \ge x_0 + x_{fed} \wedge -(\phi - \Phi_b) \le \xi' \le 0 \wedge \Delta\omega \le 0$ $g_6 \triangleq 0 \le \xi'^{+} \le \Phi_b$ $g_8 \triangleq x_s \le x_0$
$I_3 \triangleq \{\boldsymbol{x} \mid i_g = 0$	$g_7 \triangleq 0 \le \xi'^{+} \le \Phi_b$ $g_9 \triangleq x_s \le x_0 + x_{fed} \wedge \Phi_b \le \xi'^{+} \le \phi$ $g_{10} \triangleq x_s \ge x_0 + h_t \wedge \Delta\omega = 0$
$I_4 \triangleq \{\boldsymbol{x} \mid \omega_s = \omega_g \wedge x_s = x_0 + h_t$	

During the free fly state, the actuator force alone acts on the sleeve, and the gearbox losses are ignored, so there are no acting torques. According to the forces and torque balance, the dynamics of the sleeve and gearinsidel_1 are described according to Eq. (22)-(24):

$$m\ddot{x}_s = F_{act} \quad (22)$$
$$J\ddot{\theta}_s = 0 \quad (23)$$
$$J\ddot{\theta}_g = 0 \quad (24)$$

A back-end stop is included in this state dynamic to stop the sliding sleeve if it bounces back a distance larger than the axial gap.

During the face impact state, the actuator force keeps acting on the sleeve. Moreover, there is a contact force, and friction torque between the teeth' faces. Thus, the dynamics during $l_2$are described according to Eq. (25) - (27):

$$m\ddot{x}_s = F_{act} - F_c \quad (25)$$
$$J\ddot{\theta}_s = \mu r(F_c - F_{act})sign(\Delta\omega) \quad (26)$$
$$J\ddot{\theta}_g = -\mu r(F_c - F_{act})sign(\Delta\omega) \quad (27)$$

During the side impact state, the actuator force only acts on the sliding sleeve, and a contact torque is present between the gear and the sleeve teeth' sides. Thus, the dynamics during $l_3$are described according to Eq. (28) - (30):

$$m\ddot{x}_s = F_{act} \quad (28)$$
$$J\ddot{\theta}_s = T_c \quad (29)$$
$$J\ddot{\theta}_g = -T_c \quad (30)$$

A front-end stop is included in this state dynamic to stop the sliding sleeve when it reaches the final axial position.

4. Model Validation

Our developed dynamic model has been validated with two published works. Firstly it is validated with Bóka's work[18] at a low mismatch speed and according to the AMT parameters listed in[40] at the first gear. Figure 11 shows that the present model probability values agree with Bóka's analytical results and agree with the experimental statistic validation.

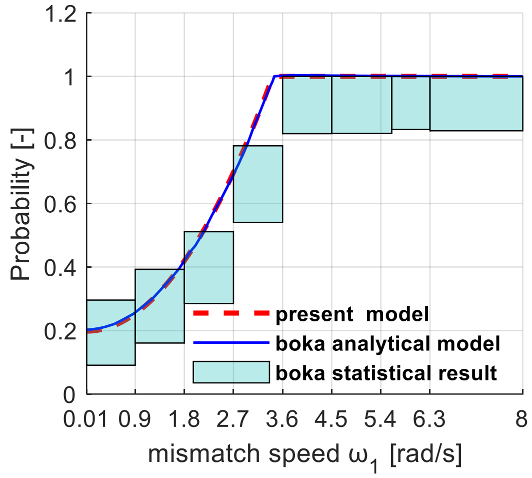

Figure 11. Model validation with Bóka[18]

Secondly, Jasný[19] performed multi-body simulation using MSC ADAMS and built an optimized model based on experimental results. One of the cases he considered is a successful gearshift without face impact, which is employed for validation. However, he used 5^o chamfered tooth side geometry and no backlash between the teeth. This work considers tooth geometry with no chamfers and with backlash, so Jasný's geometry has been adapted to this work.

The 5^o chamfer is equivalentto10^o backlash at the teeth tip, so, the teeth are considered flat with 10^o backlash. This will not alter the results since we consider a free face-contact case. The other geometry parameters are kept the same. The same initial conditions and the force time-varying profile are applied to the present model.

Figure 12 shows that the present model and Jasný's have identical position trajectories even though there is a time-varying force profile. Also, the model could successfully detect the face impact locations, so the present model has a free face impact gearshift process. The multi-body results and the simulation differ at the end position due to the difference in contact model definition.

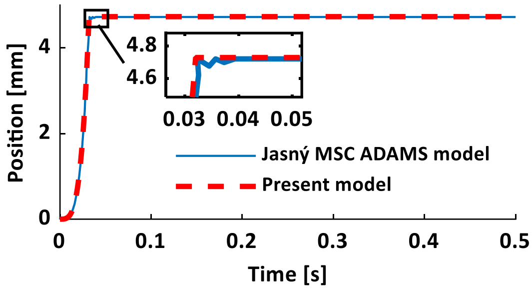

Figure 12. Model Validation with Jasný[19],$\xi_0=0^o$, and $\Delta\omega_0=50$ *RPM*

5. Simulation Results

The developed HA model is simulated on Simulink state flow machine,using*ode23tb* solver with an absolute tolerance of 10^{-9}[44]. The simulation parameters are summarized in Table 3. The impact model parameters *k* and *d* are chosen sothe system is over-damped.

Table 3. Simulation parameters

Parameters	Value	Parameters	Value
Z	10 [-]	Φ_b	5°
x_0	10 mm	x_{fed}	0.5 mm
h_t	5 mm	r	47.3 mm
k	3×10^9 Nm	d	3×10^5 Ns/m
m	6 kg	J_g	0.2 kgm^2
F_{act}	150 N	μ	0.1 [-]

Figure 13 shows the dynamic response for the system simulated by the developed HA model. The developed model could capture all the dynamic characteristics during all four stages. The curve for x_s shows that the sliding sleeve freely moves during stage *1*, and neither axial impact force spikes nor side impact torque spikes appear on the curve for F_c or T_c before *0.02s, respectively*. Moreover, the mismatch speed stays unchanged since the gearbox losses are not described. This agrees with the dynamics described in l_1. At *0.02s*, the sleeve is at $x_{s,0}$ positions, so the system enters stage *2*, as the stage curve in Figure 13shows.

Moreover, the guard $g_1$is satisfied as the curve for *g* shows, so the dynamics shifts from l_1 to l_2. Here a distinction must be made between the dynamics l_i and the stages. The l_1 dynamics can happen both in stages *2* and *3*. If the system is in stage *2* and a tooth on the sleeve meets the tangential gap (or backlash) on the gear, there is no face impact, and the dynamics are described according to l_1 and not according to l_2.

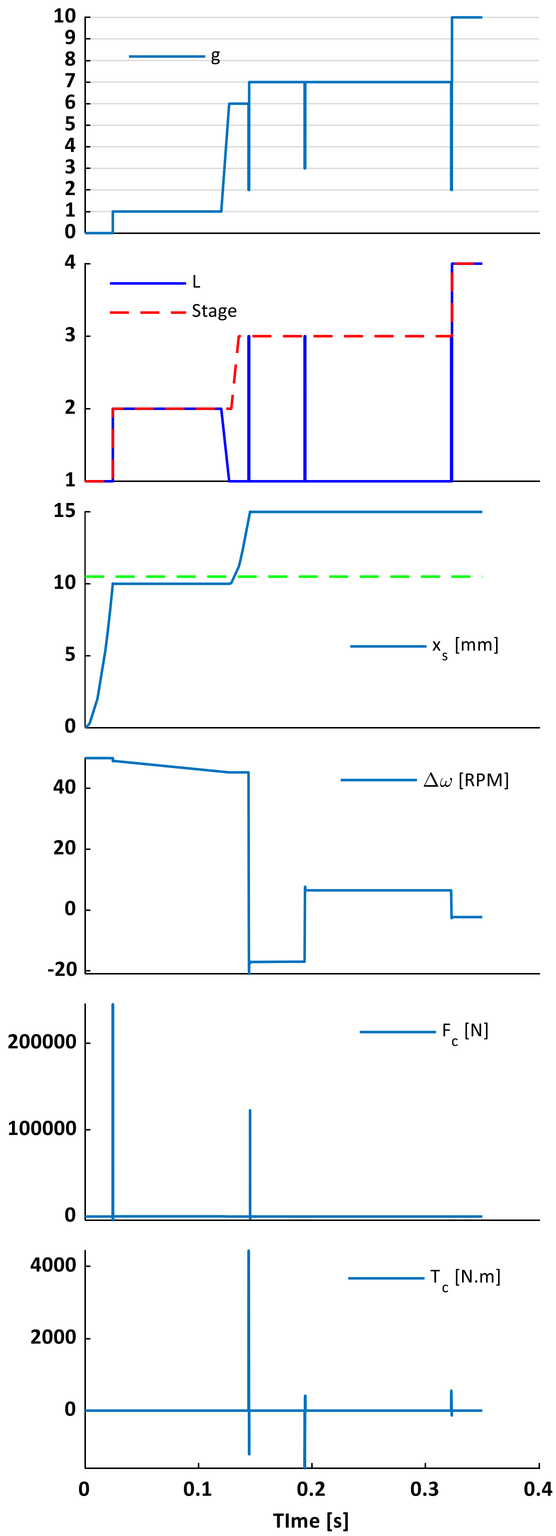

Figure 13. Case 1: HA model simulation for successful engagement case with face impact

The same applies to stage *4*; when a tooth on the sleeve moves within the backlash region in the gear, there is no side impact, and the dynamics are described according to l_1. Stage 2 starts, and axial impact force spikes appear, but no side impact torque spikes appear. Moreover, the mismatch speed decreases due to the teeth's face friction which agrees with the dynamics in l_2. The sliding sleeve stops due to the face impact and then continues to move at

0.128s, when *g* goes from *1* to *6* and *l* goes from *2* to *1* since the sleeve flies freely.

The sleeve continues the motion until it passes the overlap distance (green dashed line) at *0.133s*where stage *3* starts as the stage curve shows. However, the system enters l_3 at 0.*144s* when g_2 is satisfied, as the curve for *l* and *g* shows; even though the sleeve passed the overlap distance, it is still moving within the backlash region, so, the sleeve still flies freely and the system remained in l_1 untilg_2 is satisfied and the system goes intol_3. In stage *3*, the face impact force spikes disappear, and the side impact torque spikes start to appear. Moreover, the mismatch speed is synchronized due to the side impacts.

The system remains inl_3 for a short time due to the short impact time and then moves backtol_1 wheng_7 is satisfied. Then, a following side impact happens at*0.19s*, wheng_3 is satisfied, and the system moves to l_3. These side impacts are clear from the mismatch speed Δω curve when there is a sudden change in *Δω*.

At *0.32s*, a third side impact occurs, then the mismatch speed is synchronized, and since the sliding sleeve has already reached its final position, the system enters stage 4.

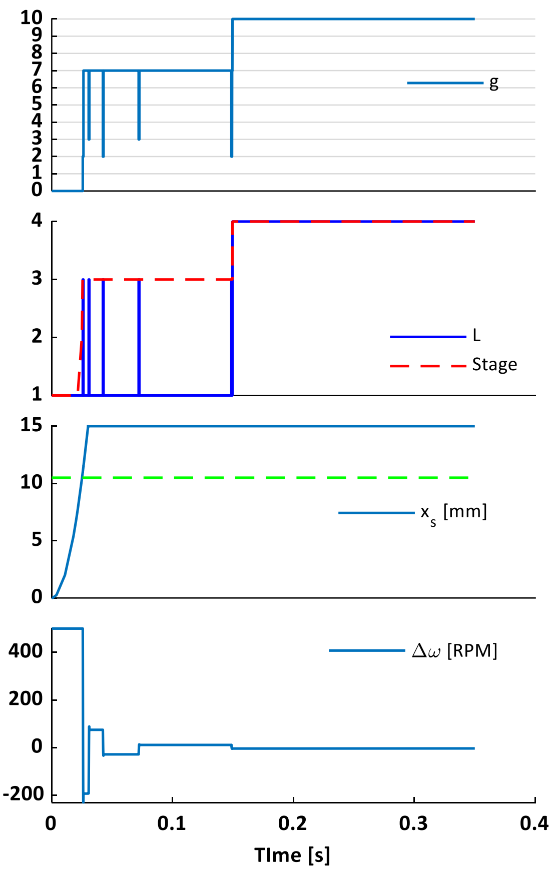

Figure 14. Case 2: HA model simulation for successful engagement case without face impact

Figure 14 shows a case for successful engagement but without face impact. The system has been simulated with $\Delta\omega_0$ of *500 RPM*. The curve for *g* shows that *g* goes from *0* to *2*, so that, *l* goes directly from *1* to *3*. This agrees with *the* x_s *curve, which* shows that the sleeve was flying freely until it reached its final position $x_{s,f}$ at *15 mm* without being stopped by the face impact. At *0.025s*, the sleeve passes the overlap distance at *10.5mm*, and the system enters stage 3. Then, g_2 is satisfied at *0.026s* and the system shift from l_1 to l_3, where the first side impact happens, as clearly seen from the sudden change in the mismatch speed curve at this time. The system stays for a short time at $l_3$then it moves back tol_1 wheng_7 is satisfied. The gear and sleeve go into several side impacts, and the system goes between l_1 and l_3. Afterward, the system shifts to stage *4* at *0.15s* when*Δω* is synchronized, andg_{10} is satisfied,

In Figure 13 and Figure 14, the contact model parameters are set to bean overdamped system, so the sleeve does not bounce back at the face impact position or when it reaches its final position. However, in Figure 15, the contact model parameters are set to be an underdamped system, where the damping is reduced to $3\times10^2 Ns/m$. The system was simulated with the same parameters as in Figure 14, except for the damping. So, Figure 14 and Figure 15have the same response before *0.026s*. However, when the sleeve reaches its final position in Figure 15, it bounces back due to the end stop, where a face impact occurs, and the sleeve bounces back because the system is underdamped. At *0.035s*, the sleeve bounces back beyond the impact position$x_{s,0}$, *10 mm*, before the actuator can move forward again. At *0.076s*, the sleeve reaches the impact position again when *g* goes from *7* to *1*, then bounces back several times where *g* goes between *1* and *8*, while *l* goes between *1* and *2*. When *g* is *1* and *l* is *2*, the system response has spikes, as seen from *g* and *l* curves, since the impact time is very short. After several attempts, the sleeve could pass stage *1* to stage *3* directly at*0.25s*, when *g* changes from *8* to *2* and *l* from *1* to *3*, but it bounces back again at its final position $x_{s,f}$ several times. After this time, several side impacts occur, as seen from *g* and *l* curves where they alternate between *2*, or *3* and *7*, and between *1* and *3*, respectively but the mismatch speed is not synchronized. Even though the sleeve reached its final position, the system did not enter stage 4, as *g* and *l* did not reach *10* and *4*, respectively. The sleeve did not stay at the final position and the mismatch speed is not synchronized.

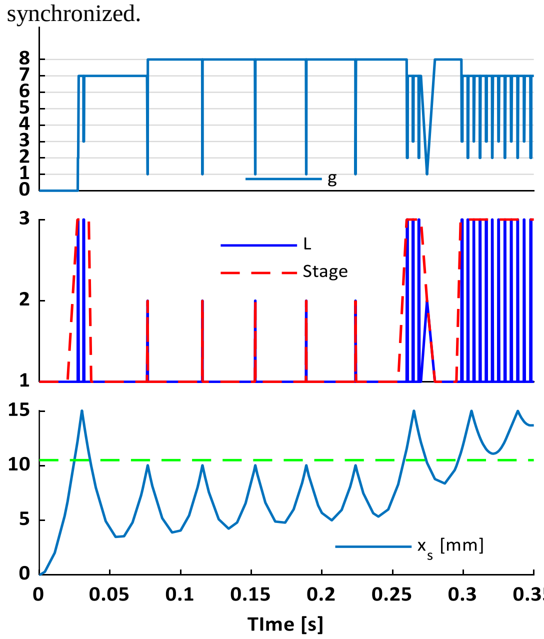

Figure 15. Case 3: HA model simulation for unsuccessful engagement case with underdamped contact

6. Conclusion

In this work, HA technique is employed to overcome the drawbacks of CT technique. HA model is formed to describe the dog clutch dynamics during the gearshift process. The role of HA is to integrate the dynamics of the discrete state into one analog model to capture the continuous system's dynamics.

Three gearshift cases are considered to verify the HA model, and Simulink simulation showed that the HA model could capture the continuous states' dynamics inside each discrete state and the state transition and dynamics behavior agrees with the formed HA model. This is clearly seen in the agreement of *l* with g curves from one side and the agreement of position, and mismatch speed trajectories with *l* curve from another side

Currently, a test rig prototype for sequential transmission is being built at our department. In future research, another dynamic model describing the whole test rig is developed to estimate the unknown system parameters based on the measurements, then, the calibrated dynamic model will be validated. Later, this HA model will be integrated with a shifting mechanism model to design a controller for the shifting mechanism's actuator to guarantee a successful gearshift process without face impact.

References

[1] O. Al-Oran, F. Lezsovits, A. Aljawabrah, "Exergy and energy amelioration for parabolic trough collector using mono and hybrid nanofluids". Journal of Thermal Analysis and Calorimetry, Vol. 140, No. 3, 2020, 1579-1596.

[2] A. Qazi, F. Hussain, N. A. Rahim, G. Hardaker, D. Alghazzawi, K. Shaban, K. Haruna, "Towards sustainable energy: a systematic review of renewable energy sources, technologies, and public opinions". IEEE access, Vol. 7, 2019, 63837-63851.

[3] R. A. Burgelman, A. S. Grove, "Toward Electric Cars and Clean Coal: A Comparative Analysis of Strategies and Strategy-Making in the US and China". 2010,

[4] M. A. Mallouh, B. Denman, B. Surgenor, B. Peppley, "A study of fuel cell hybrid auto rickshaws using realistic urban drive cycles". Jordan Journal of Mechanical and Industrial Engineering, Vol. 4, No. 1, 2010, 225-229.

[5] D. Liu, S. Li, H. Liu, "Experimental Study on Formaldehyde Emission from Environmental Protection and Energy-Saving Alcohol Fuel for Vehicles". Jordan Journal of Mechanical and Industrial Engineering, Vol. 15, No. 1, 2021, 1-6.

[6] R. J. Socin, L. K. Walters, "Manual transmission synchronizers". SAE Transactions, Vol. 77, 1968, 31-65.

[7] L. Lovas, D. Play, J. Márialigeti, J.-F. Rigal, "Modelling of gear changing behaviour". Periodica Polytechnica Transportation Engineering, Vol. 34, No. 1-2, 2006, 35-58.

[8] L. Lovas, D. Play, J. Márialigeti, J.-F. Rigal, "Mechanical behaviour simulation for synchromesh mechanism improvements". Proceedings of the Institution of Mechanical Engineers, Part D: Journal of Automobile Engineering, Vol. 220, No. 7, 2006, 919-945.

[9] D. T. VIER, S. J. KOWAL, "Composite friction and dog clutch." USA, 10060485, 2018.

[10] I. Shiotsu, H. Tani, M. Kimura, Y. Nozawa, A. Honda, M. Tabuchi, H. Yoshino, K. Kanzaki, "Development of High Efficiency Dog Clutch with One-Way Mechanism for Stepped Automatic Transmissions". International Journal of Automotive Engineering, Vol. 10, No. 2, 2019, 156-161.

[11] B. Chen, J. Guo, M. Yan, F. Wang, F. Liu, "Study on a Ni-P-nano TiN composite coating for significantly improving the service life of copper alloy synchronizer rings". Applied Surface Science, Vol. 504, 2020, 144116.

[12] K. Barathiraja, G. Devaradjane, A. Bhattacharya, V. Sivakumar, V. Yadav, "Automotive Transmission Gearbox Synchronizer Sintered Hub Design". Engineering Failure Analysis, Vol. 107, 2020, 104213.

[13] A. Myklebust, L. Eriksson, "Modeling, observability, and estimation of thermal effects and aging on transmitted torque in a heavy duty truck with a dry clutch". IEEE/ASME transactions on mechatronics, Vol. 20, No. 1, 2014, 61-72.

[14] B. Gao, H. Chen, Y. Ma, K. Sanada, "Design of nonlinear shaft torque observer for trucks with Automated Manual Transmission". Mechatronics, Vol. 21, No. 6, 2011, 1034-1042.

[15] A. Aljawabrah, L. Lovas, "Shiftability Study of a Dog Clutch". VII Gépészeti Szakmakultúra Konferencia, Budapest, Hungary, 2022

[16] G. Bóka, J. Márialigeti, L. Lovas, B. Trencséni, "External synchronization strategies for automated mechanical transmissions with face dog clutch and countershaft brake". Scientific Bulletin Series C: Fascicle Mechanics, Tribology, Machine Manufacturing Technology, Vol. 23, 2009, 75-80.

[17] A. Szabo, T. Becsi, S. Aradi, "Linear parameter-varying control of a floating piston electro-pneumatic actuator". IEEE 24th International Conference on Intelligent Engineering Systems (INES), Budapest, Hungary, 2020.

[18] G. Bóka, J. Márialigeti, L. Lovas, B. Trencséni, "Face dog clutch engagement at low mismatch speed". Periodica Polytechnica Transportation Engineering, Vol. 38, No. 1, 2010, 29-35.

[19] M. Jasný, M. Hajžman, G. Achtenová, "Multi-body simulation of dog clutch engagement". 45. mezinárodní vědecká konference kateder dopravních, manipulačních, stavebních a zemědělských strojů, Zborovska, Czech Republic, 2019.

[20] J. Ruan, P. Walker, N. Zhang, "A comparative study energy consumption and costs of battery electric vehicle transmissions". Applied Energy, Vol. 165, 2016, 119-134.

[21] K. Kwon, J. Jo, S. Min, "Multi-objective gear ratio and shifting pattern optimization of multi-speed transmissions for electric vehicles considering variable transmission efficiency". Energy, Vol. 236, 2021, 121419.

[22] A. Esser, T. Eichenlaub, J.-E. Schleiffer, P. Jardin, S. Rinderknecht, "Comparative evaluation of powertrain concepts through an eco-impact optimization framework with real driving data". Optimization and Engineering, Vol. 22, No. 2, 2021, 1001-1029.

[23] T. K. Bera, K. Bhattacharya, A. K. Samantaray, "Evaluation of antilock braking system with an integrated model of full vehicle system dynamics". Simulation Modelling Practice and Theory, Vol. 19, No. 10, 2011, 2131-2150.

[24] P. D. Walker, Y. Fang, N. Zhang, "Dynamics and control of clutchless automated manual transmissions for electric vehicles". Journal of Vibration and Acoustics, Vol. 139, No. 6, 2017, 061005 (13 pages).

[25] J.-q. Xi, L. Wang, W.-q. Fu, W.-w. LIANG, "Shifting control technology on automatic mechanical transmission of pure electric buses". Transactions of Beijing Institute of Technology, Vol. 1, 2010, 42-45.

[26] H. Liu, Y. Lei, Z. Li, J. Zhang, Y. Li, "Gear-shift strategy for a clutchless automated manual transmission in battery electric vehicles". SAE International Journal of Commercial Vehicles, Vol. 5, No. 2012-01-0115, 2012, 57-62.

[27] J. Li, P. Sheng, K. Shao, "Optimization of Clutchless AMT Shift Control Strategy for Electric Vehicles". Jordan Journal of Mechanical and Industrial Engineering, Vol. 14, No. 1, 2020, 109 - 117.

[28] A. Eßer, J. Mölleney, S. Rinderknecht, "Potentials to reduce the Energy Consumption of Electric Vehicles in Urban Traffic". VDI-Berichte, Darmstadt, Germany, 3180924012, Vol. 2401, 2022.

[29] Q. Zhang, Y. Wang, W. Lin, Y. Luo, X. Wu, "Contact Mechanics Analysis and Optimization of Shape Modification of Electric Vehicle Gearbox". Jordan Journal of Mechanical and Industrial Engineering, Vol. 14, No. 1, 2020, 15-24.

[30] Q. Pan, J. Zhang, "Electromechanical Coupling Model of AC Asynchronous Motor Drive System Based on Multiscale Method". Jordan Journal of Mechanical and Industrial Engineering, Vol. 15, No. 1, 2021, 73 -82.

[31] T. A. Henzinger, The theory of hybrid automata. In: M. K. Inan and R. P. Kurshan, editors. Verification of digital and hybrid systems. Berlin, Germany: Springer, 2000, p. 265-292.

[32] J.-F. Raskin, An introduction to hybrid automata. In: D. Hristu-Varsakelis and W. S. Levine, editors. Handbook of networked and embedded control systems. Basel, Switzerland: Birkhäuser Boston, 2005, p. 491-517.

[33] R. Alur, C. Courcoubetis, T. A. Henzinger, P.-H. Ho, Hybrid automata: An algorithmic approach to the specification and verification of hybrid systems. In: R. L. Grossman, A. Nerode, A. P. Ravn, and H. Rischel, editors. Hybrid systems. Heidelberg, Berlin, Germany: Springer, 1992, p. 209-229.

[34] J. Lygeros, K. H. Johansson, S. N. Simic, J. Zhang, S. S. Sastry, "Dynamical properties of hybrid automata". IEEE Transactions on automatic control, Vol. 48, No. 1, 2003, 2-17.

[35] H. Fu, G. Tian, Q. Chen, Y. Jin, "Hybrid automata of an integrated motor-transmission powertrain for automatic gear shift". American Control Conference, San Francisco, California, USA, 2011.

[36] H. Chen, S. Mitra, "Synthesis and verification of motor-transmission shift controller for electric vehicles". 5th ACM/IEEE International Conference on Cyber-Physical Systems (ICCPS), Berlin, Germany, 2014.

[37] Z. Lu, H. Chen, L. Wang, Y. Zeng, X. Ren, K. Li, G. Tian, "Gear-shifting control of non-synchronizer electric-driven mechanical transmission with active angle alignment". Optimal Control Applications and Methods, 2021, 322-338.

[38] Z. Yuanfan, C. Hongxu, W. Lijun, T. Guangyu, Z. Weibo, "Modeling and control of gear shifting of a non-synchronizer motor-transmission drive system". Journal of Tsinghua University (Science and Technology), Vol. 60, No. 11, 2020, 910-919.

[39] A. Aljawabrah, L. Lovas, "Test rig for automated transmission with dog clutches". GÉP, Vol. 72, No. 3-4, 2021, 5-8.

[40] G. BÓKA, "Shifting Optimization of Face Dog Clutches in Heavy Duty Automated Mechanical Transmissions [Dissertation]". Budapest University of Technology and Economics, 2011,

[41] M. Ahmad, K. A. Ismail, F. Mat, "Impact models and coefficient of restitution: A review". ARPN Journal of Engineering and Applied Sciences, Vol. 11, No. 10, 2016, 6549-6555.

[42] K. Li, A. P. Darby, "Modelling a buffered impact damper system using a spring–damper model of impact". Structural Control and Health Monitoring, Vol. 16, No. 3, 2009, 287-302.

[43] M. Nagurka, S. Huang, "A mass-spring-damper model of a bouncing ball". American control conference, Boston, MA, USA, 2004.

[44] M. Hosea, L. Shampine, "Analysis and implementation of TR-BDF2". Applied Numerical Mathematics, Vol. 20, No. 1-2, 1996, 21-37.